# Novel non-noble metal electrocatalysts synthesized by heat-treatment of iron terpyridine complexes for the oxygen reduction reaction

Jiatang Wang, Shang Li*, Guangwen Zhu, Wei Zhao, Ruixin Chen, Mu Pan

*State Key Laboratory of Advanced Technology for Materials Synthesis and Processing, Wuhan University of Technology, Wuhan 430070, PR China*

## HIGHLIGHTS

- 2,6-Bis(2-pyridy)-pyridine as N-containing ligand to synthesize new ORR catalysts.
- The activity of catalyst might be from pyridinic nitrogen and graphitic nitrogen.
- Maximum power density of PEMFC achieved 0.08 W cm$^{-2}$ at 60 °C without backpressure.

## ABSTRACT

2,6-Bis(2-pyridyl)-pyridine (TPY) is used as a ligand to prepare iron-TPY (Fe-TPY) complexes for the development of a new oxygen reduction reaction (ORR) catalyst. The prepared Fe-TPY complexes are then treated at temperatures of 600 °C, 700 °C, 800 °C and 900 °C to obtain Fe–N/C catalysts. The molar ratio of Fe/TPY and Fe loadings are also optimized. The results show that the catalyst with Fe loading of 5 wt % obtained via heat-treatment of the Fe-TPY/C (mole ratio of Fe/TPY is 1:5) complex at 800 °C is the most active ORR catalyst. The overall electron transfer number for the catalyzed ORR is determined to be 3.7. The result of X-ray photoelectron spectroscopy (XPS) indicates that the atomic N contributing to the ORR activity of Fe–N/C catalyst may be from the pyridinic and graphitic nitrogens formed during heat-treatment. At a cell voltage of 0.21 V, the single cell test results show a current density of 0.38 A cm$^{-2}$ with a power density of 0.08 W cm$^{-2}$ at 60 °C without backpressure, indicating that this catalyst has the potential to be used as a non-noble catalyst in a proton exchange membrane fuel cell.

© 2013 Elsevier B.V. All rights reserved.

## 1. Introduction

Over the past decades, proton exchange membrane fuel cells (PEMFC) have attracted great efforts because of its advantages of high-energy density, high power density, high-energy conversion efficiency, low temperature of operation and environmental benefits. However, the major barrier to the commercialization of PEMFC is the high costs of Pt based catalysts and their insufficient stability [1,2]. With respect to the high cost, reducing Pt loading or completely replacing Pt using non-noble metal catalysts is considered to be the short and long term sustainable solution for PEMFC commercialization respectively [3].

Due to the slow kinetics of the oxygen reduction reaction (ORR) on Pt catalyst, the cathode of PEMFC requires much more Pt than the faster anodic hydrogen oxidation reaction (HOR). As a consequence, the ORR has a greater impact than the HOR, thus making the ORR is the dominant limiting factor in fuel cell performance [4–6]. Therefore, tremendous progress has been made in the study of the non-noble metal catalysts on cathodes for the ORR including Co or Fe-based macrocyclic compounds [5,7–10], transition metal chalcogenides [11,12], nitrogen-doped carbon nanotubes [13,14], nitrogen-doped ordered mesoporous carbon [15,16] and even nitrogen-doped graphene [17,18]. Among them the most promising catalysts for the ORR in acidic medium are heat-treated Fe and Co based nitrogen complexes. The performance of these catalysts is directly related to their preparation conditions including the synthesis method, metal precursor, ligand structure, carbon support and heat-treatment [19]. Nitrogen (N)-containing precursors play a significant role during the M-N$_x$/C synthesis in order to form an active catalyst. N-containing chemicals such as polyacrylonitrile, ethylenediamine, tripyridyl triazine (TPTZ), NH$_3$, acetonitrile, polyaniline (PANI), phthalocyanine, ploypyrrole, phenanthroline and nitrogen groups on a modified carbon support have been found to be effective nitrogen sources for M-N$_x$/C catalyst preparation [2,5–10,16,20–26]. It seems fairly certain that the activity of this kind of catalyst is related to its nitrogen content and

* Corresponding author. Tel.: +86 27 8765 1837x8611; fax: +86 27 8787 9468.
  E-mail address: lishang@whut.edu.cn (S. Li).

type of ligands [15]. Thus far, the most active ORR catalysts were synthesized by Zelenay's group [5] using PANI as a ligand to form Fe−PANI and FeCo−PANI complexes, which were then heat-treated in an inert atmosphere of nitrogen gas for 1 h. The obtained PANI−FeCo−C catalyst had the highest maximum power density (0.55 W cm$^{-2}$) and it displayed very promising performance stability in fuel cell testing. These authors summarized that the high activity and enhancing stability of PANI-derived catalysts might be due to the formation of graphene sheets during the heat-treatment which were somewhat disordered and had a larger d-spacing of the (002) basal planes. This may facilitate incorporation of nitrogen into the graphitic structure and thereby enhance the number of active sites. Moreover, the graphitization of the onion-like nano-shells and nanofibers as well as the presence and formation of graphene sheets throughout the PANI-derived catalysts may also enhance the electronic conductivity and corrosion resistance of the carbon based catalysts. They also indicated that the identity of the active oxygen reduction site, along with a better understanding of the reaction mechanism, remains to be determined. In our previous work [10,19] carbon-supported Fe$_1$Co$_1$−N/C and Fe−N/C catalysts were synthesized using tripyridyl triazine (TPTZ) as the complex ligand. The performance of these catalysts was similar to that of the carbon-supported Co−PPY catalyst developed by Zelenay's group [27]. This Fe-TPTZ based catalyst catalyzed the ORR process mainly through a 4-electron transfer pathway that produced water. It was also found that the pyridinic nitrogen which consists of one nitrogen atom at the edge of a graphene layer and the aromatic type nitrogen on the central aromatic ring in the TPTZ molecule might predominantly contribute to the catalytic activity of these catalysts. In this paper, we report the synthesis and exploration of potential PEMFC catalysts from a heterocyclic complex called 2,6-Bis(2-pyridy)-pyridine (TPY) and used as a nitrogen-containing precursor. The unique feature of the TPY is that it has three pyridine rings that are usually close to being co-planar connected to each other through sigma ($\sigma$) bonding and are well known to form complexes with various metal ions [28]. In the solid state the three pyridine rings exhibit transoid configurations about the interannular carbon−carbon bonds and three possible configurations are shown in Fig. 1 [29]. When a TPY ligand is bonded to a metal it can isomerise to a cis-configuration shown in Fig. 1b, and cis−cis-configuration as shown in Fig. 1c.

The coordination chemistry of the TPY ligand has attracted interest from many chemists since its synthesis was first reported almost 70 years ago [29]. Ligand TPY has been reacted with many metals to prepare complexes used as catalysts and in the detection of transition metals. In terms of catalyst, the focus is on Ru, Fe, Co, Pt, Cu, Ni or Mn based TPY complexes which showed effective catalytic activity towards photo-catalysis, cyclopropanation of alkenes, oxidation of alcohols, reduction of $CO_2$, NO, $NO_2$ and the cleavage of deoxyribose nucleic acid (DNA) [29−35]. Materials Visualizer for polymers run by the Materials Studio Modeling 5.0 package (2001−2009 Accelrys Software Inc.) was used to carry out our modeling calculation studies. TPY could form a complex with Fe iron, and the proposed structure of this
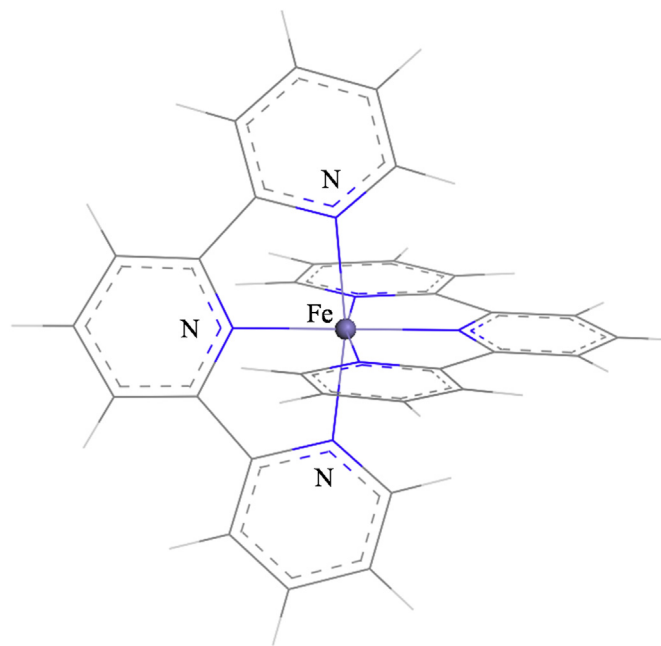


**Fig. 2.** The proposed structure of Fe−TPY complex.

Fe−TPY complex is shown in Fig. 2. We calculated the Fe−TPY complex by the incidental measurements tools within the Materials Studio modeling software, the bond length between the Fe ion and the nitrogen on the central aromatic ring of the TPY molecule is 2.086 Å, while that between the Fe ion and the pyridinic nitrogen at the edge of the molecule is 2.159 Å, indicating that the Fe ion bonds more easily with the pyridinic nitrogen on the central aromatic ring than to the nitrogen on the edge of the aromatic rings.

According to the Fe−TPTZ compound synthesized by Bezerra et al. [19] whose structure is similar to the Fe−TPY complex, it was believed that the bonding between the Fe ion and the central nitrogen in TPTZ is essential for the formation of catalytic activity sites for ORR. The Fe−TPY complex should be activated towards ORR after heat-treatment. Therefore, in this paper, the Fe−TPY complex was used as a nitrogen-containing precursor to form carbon-supported catalysts for PEMFC applications. Heat-treatment temperature (from 600 to 900 °C), Fe loadings (3.0, 4.0, 5.0, 6.0 and 7.0 wt%), and the mole ratio of Fe/TPY (1:2.1, 1:4, 1:5, 1:6 and 1:8) were optimized to achieve active ORR electrocatalysts (Fe−N/C). X-ray diffraction (XRD) technique was applied to analyze catalyst structure and composition. The catalyst morphologies were characterized by high resolution transmission electron microscopy (HRTEM) and X-ray photoelectron spectroscopy (XPS) was employed to examine the surface chemical composition of Fe−N/C catalyst. The ORR activities were studied in an acidic medium using cyclic voltammetry (CV) and rotating disk electrode (RDE) techniques. A PEMFC with a cathode catalyzed by this catalyst was constructed. The
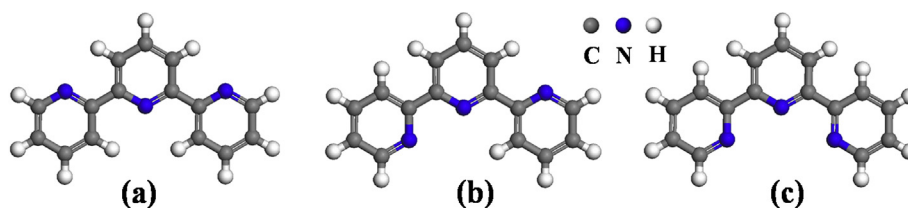


**Fig. 1.** The configuration of the ligand TPY.

performance of this single fuel cell demonstrated that this carbon-supported Fe−N catalyst is a potential cathode catalyst for PEMFC.

## 2. Experimental

### 2.1. Chemicals

TPY ($\geq$97%) was purchased from Alfa Aesar and used as received. Black Pearls 2000 with BET surface area of about 1500 $m^2$ $g^{-1}$ was employed as the catalyst support and obtained from Cabot. The compound $(NH_4)_2Fe(SO_4)_2 \cdot 6H_2O$ was purchased from Sinopharm Chemical Reagent Co. Ltd. (China). Nitrogen and Oxygen gases were supplied in cylinders with 99.999% purity. The experimental re-agents were of analytic grade and used as received without further purification. The solutions were prepared using ultra pure water obtained from a Lab. ultra pure water filter system with a resistivity $\geq$18 M$\Omega$ $cm^{-1}$.

### 2.2. Catalyst preparation

During catalyst synthesis, the carbon support suspension was obtained by mixing 1 g Black Pearls 2000 with a 3% ethanol solution at 60 °C under constant stirring. To synthesize the carbon-supported Fe-TPY complex, 4 mL of 0.224 M aqueous solution of $(NH_4)_2Fe(SO_4)_2 \cdot 6H_2O$ and 5 mL of 0.376 M ethanol solution of TPY were slowly added to the carbon support suspension and stirred for at least 20 h. The mixture was then dried in an oven at 100 °C overnight forming a black Fe-TPY/C powder. The Fe content of this powder was expected to be approximately 5.0 wt% and the mole ratio of Fe to TPY was 1:2.1. After being ground in a mortar, the powder was then placed for 1 h in a tube furnace under $N_2$ with a flow rate of 150 mL $min^{-1}$ to remove any residual air before the temperature was increased. After which the tube furnace was adjusted to increase the temperature at a ramping rate of 5 °C $min^{-1}$ until the desired heat-treatment temperature was reached and the temperature was then held at this for 2 h. The final carbon-supported catalyst (expressed as 5 wt% Fe−N/C) was obtained after the tube furnace was cooled down to room temperature. The heat-treatment temperatures were 600 °C, 700 °C, 800 °C and 900 °C. The same procedure was used to synthesize catalysts with different mole ratios of Fe/TPY (1:4, 1:5, 1:6 and 1:8) which were varied by changing the volume of the aqueous and ethanol solutions and Fe loadings (3.0, 4.0, 6.0, and 7.0 wt%) which is the weight ratio of Fe and Black Pearls 2000 (1.000 g in all experiments) and varied only by changing the volume of the aqueous component of $(NH_4)_2Fe(SO_4)_2 \cdot 6H_2O$.

### 2.3. Physical and surface characterization of the catalysts

The structures of the catalysts were analyzed by XRD using D/Max-RB X-ray Powder Diffractometer with Cu-Ka radiation and the XRD patterns were recorded between 10° and 80° and a powder diffraction file database was used to assign the diffractograms. The morphology of the catalyst samples was analyzed using a JEM-2100F HRTEM and electronic structure of the catalyst surface analysis performed using XPS (VG Multilab 2000).

### 2.4. Preparation of the working electrodes

To prepare the working electrode, a homogeneous catalyst ink was made by mixing of 4.0 mg catalyst, 50 μL Nafion® ionomer solution (5 wt%, DuPont) and 1 mL ultra pure water. The 20 μL of catalyst ink was spread onto the surface of a glassy carbon (GC) disk electrode of geometric area 0.20 $cm^2$ with a micrometer pipette to form the catalyst layer. The catalyst loading was kept at

0.4 $mg_{catalyst}$ $cm^{-2}$. If the Fe content in the catalyst powders was different the catalyst layers formed using these different catalyst inks were expected to have different Fe loadings, even though the initial catalyst loadings had been the same.

### 2.5. Electrochemical measurements

All the electrochemical performances of Fe−N/C catalysts were measured using a conventional three-compartment electro-chemical cell in 0.5 M $H_2SO_4$ aqueous solution. Pt gauze and a saturated calomel electrode (SCE) were used as the counter and reference electrode, respectively. The SCE reference electrode was calibrated against the reversible hydrogen electrode (RHE). The working electrode was constructed with a GC disk electrode coated with Fe−N/C catalyst layer. The ORR performance was carried out using RDE technique by linear sweep voltammetry (LSV) in the potential range of −0.2 to 0.7 V (vs. SCE) with a scan rate of 5 mV $s^{-1}$ in an oxygen-saturated $H_2SO_4$ solution. CV was collected in the potential range of −0.2 to 0.7 V (vs. SCE) with a scan rate of 50 mV $s^{-1}$ in nitrogen saturated $H_2SO_4$ solution. In this paper, all the potentials were normalized to the reversible hydrogen elec-trode (RHE), all current densities were normalized to the geometric surface area of the disk electrode and all the electrochemical ex-periments were carried out at room temperature and ambient pressure.

### 2.6. Single fuel cell testing

To evaluate their activities under PEMFC operating conditions catalysts were tested in the fuel cell cathode. Single cell hardware used was made in Lab. and a Greenlight™ fuel cell test station was used for the test. The single cell was operated at 60 °C and ambient pressure. Commercial Pt/C catalyst was used at the anode. The anode side was fed by pure hydrogen with a flow rate of 0.5 L $min^{-1}$ and the cathode side was fed by pure oxygen with a flow rate of 0.8 L $min^{-1}$. Both gases were humidified with 100% relative humidity.

## 3. Results and discussion

### 3.1. Physical characterization of Fe−N/C catalysts

As described in the experimental section, XRD was employed to gain insights into the crystalline structure of the Fe−N/C catalysts heat-treated at different temperatures. In this section, the mole ratio of Fe/TPY and Fe loadings are 1:2.1 and 5 wt%, respectively. Fig. 3 shows spectra of the Fe-TPY/C complex heat-treated at four different temperatures under $N_2$ atmosphere. The wide peak at 24° corresponds to the carbon support. It is observed that the samples heat-treated at temperatures from 600 °C up to 800 °C have very similar peaks. The small peak at 35.38° may be related to the formation of metallic Fe during the complicated heat-treatment processes, which might spontaneously oxidize to Fe oxides when exposed to air at room temperature. This Fe oxide phase can be further confirmed from the XRD pattern when temperature is further increased to 900 °C, a sharp and narrow diffraction peak at 35.38° and four peaks at 30.08°, 43.02°, 57.1° and 62.7° are observed. These five peaks can be attributable to the typical $Fe_3O_4$ phases (35.42°, 30.09°, 43.05°, 56.94° and 62.52°). The de-compositions of Fe−TPY complexes during heat-treatment are believed to be complicated processes producing many species including metal-nitrogen species, metals in their metallic state and metal carbides [36]. Normally, the metallic state metals and/or metallic oxides have less catalytic activity towards the ORR. Hence, to prevent the formation of Fe oxides in the catalysts, the heat-
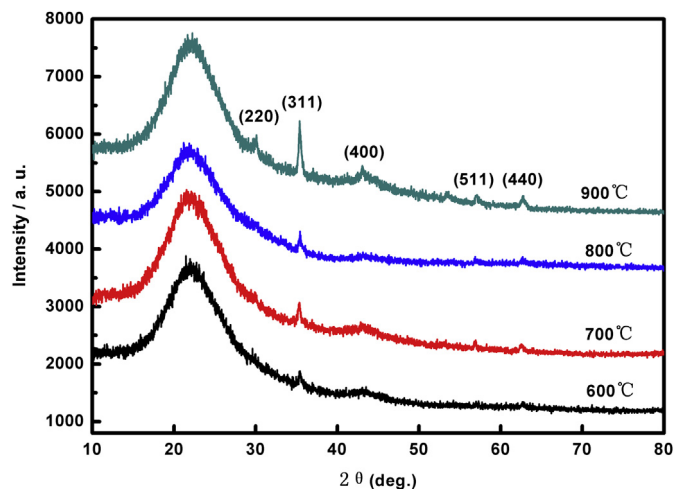
**Fig. 3.** XRD patterns for Fe–TPY/C samples after being heat-treated at 600 °C, 700 °C, 800 °C and 900 °C. Ratio of Fe/TPY and metal loading were 1:2.1 and 5.0 wt% respectively.
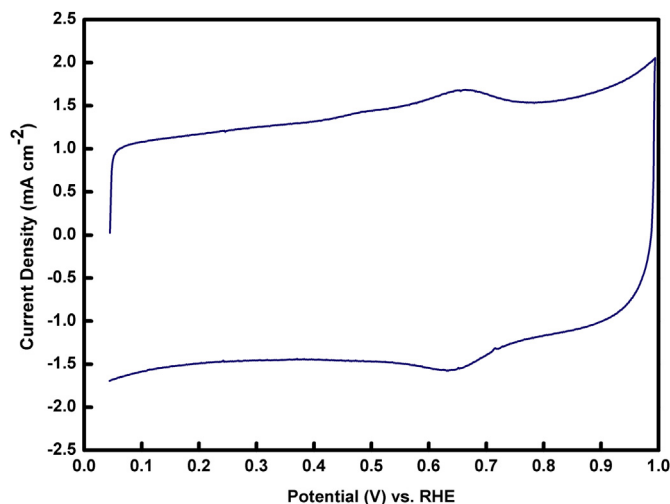


**Fig. 5.** CV of Fe–TPY/C samples heat-treatment at 800 °C. The Fe–N/C catalyst was coated on a GC electrode surface. Recorded in $N_2$-saturated 0.5 M $H_2SO_4$ solution. Fe–N/C catalyst loading: 0.40 mg cm$^{-2}$. Potential scan rate: 50 mV s$^{-1}$.

treatment temperature for Fe–N/C synthesis should not be higher than 800 °C. It could also be confirmed by Fig. 6 in which the 800 °C treated catalyst has the best ORR activity.

The HRTEM images of an Fe–N/C catalyst heat-treated at 800 °C is shown in Fig. 4. It is similar as the HRTEM micrograph of a Fe-TPTZ/C catalyst heat-treated at 800 °C [19]. It can be observed from Fig. 4a that the sizes of carbon support nanoparticles are about 30 nm. The Fe cluster mentioned in XRD section is too small to be observed in this micrograph. This is consistent with the observation from the XRD analysis shown in Fig. 3. The presence of diverse carbon nanostructures in which the well-defined graphitic carbon is surrounded by amorphous carbon are attested to as shown by the red arrows in Fig. 4b. As mentioned in the introduction, this graphitic structure formed during heat-treatment was also observed in the PANI–FeCo–C catalyst [5]. The formation of graphene sheets was correlated to the high activity and enhancing stability of PANI-derived catalysts.

### 3.2. Surface electrochemistry of Fe–N/C catalyst

Fig. 5 shows the CV of the Fe–N/C catalyst heat-treated at 800 °C recorded in $N_2$-saturated 0.5 M $H_2SO_4$ solution. A reversible redox peak at about 0.65 V (vs. RHE) is clearly observed. In our previous

research on a single Fe–N/C catalyst, we recorded a redox peak at the same position and assigned it to a redox process of Fe (II)/Fe (III) [10].

### 3.3. Effect of heat-treatment temperature on the catalytic ORR activity

Heat-treatment had a significant effect on the ORR catalytic activity of non-noble catalysts, in particular on transition metal macrocycles [36]. In order to optimize the heat-treatment temperature with respect to catalyst activity, the liner scanning voltammetries of catalysts heat-treated at 600 °C, 700 °C, 800 °C and 900 °C were tested using RDE technique. The results are shown in Fig. 6a, and ORR potentials obtained for the different catalysts at the current density of 0.5 mA cm$^{-2}$ are shown in Fig. 6b for comparison. The optimum heat-treatment temperature resulting in the highest ORR potential at that current density is 800 °C.

Although the mechanism for the effect of heat-treatment on catalytic ORR activity seems to be complicated, it is not yet fully understood. It has been recognized that heat-treatment is a necessary step in improving the ORR activity of metal-nitrogen catalysts. The main function of heat-treatment is to create active
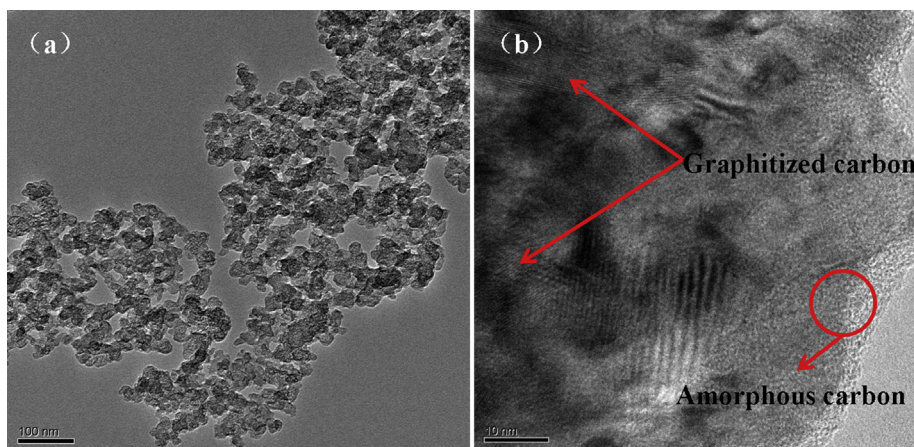


**Fig. 4.** HRTEM images of Fe–TPY/C complex after heat-treatment at 800 °C.
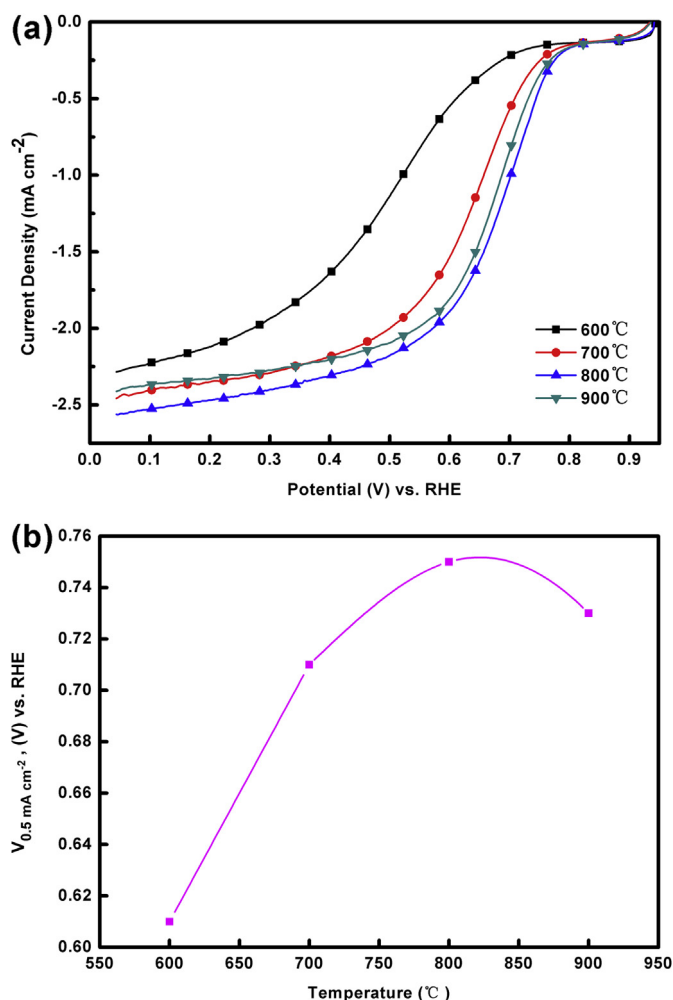
**Fig. 6.** (a) Current−voltage curves recorded on a rotating GC electrode coated with Fe− N/C catalysts heat-treated at various temperatures, as marked in the figure. Electrolyte: $O_2$-saturated 0.5 M $H_2SO_4$ solution; electrode rotating rate: 400 rpm; potential scan rate: 5 mV s$^{-1}$; Fe−N/C catalyst loading in the coating layer: 0.40 mg cm$^{-2}$. (b) ORR potentials at 0.5 mA cm$^{-2}$ as a function of heat-treatment temperature.
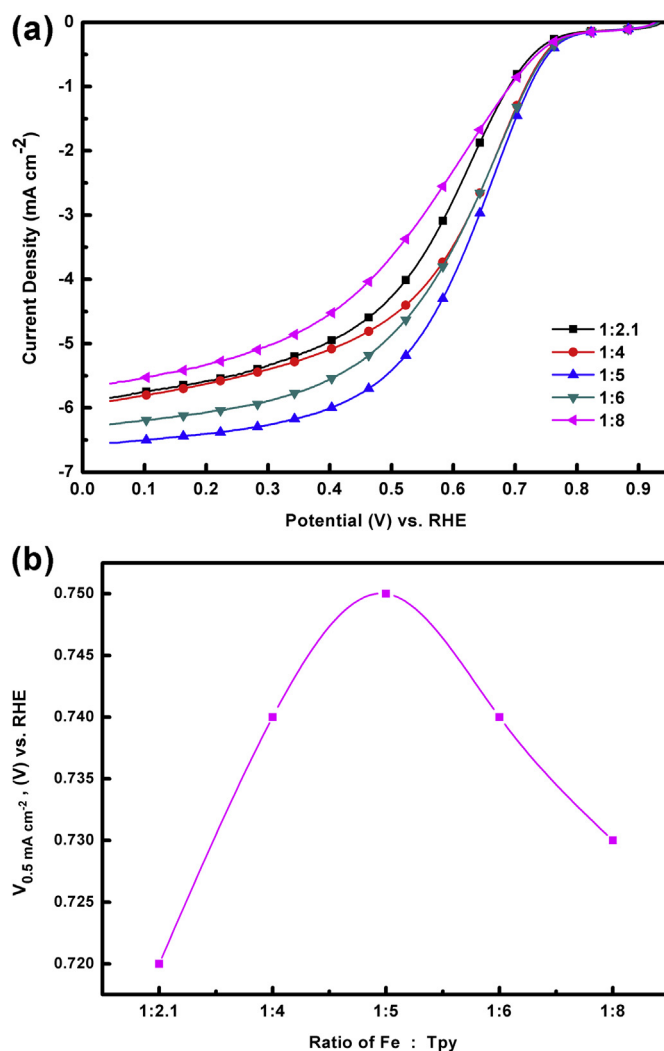


**Fig. 7.** (a) Current−voltage curves obtained on a rotating GC electrode coated with different Fe−N$_x$/C catalysts synthesized at 800 °C heat-treatment process of Fe-TPY precursor complexes with different Fe to TPY mole ratios as marked in the figure. Measurements were carried out in $O_2$-saturated 0.5 M $H_2SO_4$ solutions. Potential scan rate: 5 mV s$^{-1}$, electrode rotation rate: 2500 rpm, catalyst loading in the coating: 0.40 mg cm$^{-2}$. (b) ORR potential at 0.5 mA cm$^{-2}$ as a function of Fe to Tpy mole ratio (data taken from (a)).

sites for the ORR [36]. From 600 °C to 800 °C, the ORR activity in- creases with increasing heat-treatment temperature indicating that more possible active sites, such as Fe−N$_4$, Fe−N$_2$ or C−N groups, may be formed as the heat-treatment temperature rises. The 800 °C Fe−N$_x$ gradually converts into metal Fe and/or Fe oxides (as observed in Fig. 3) reducing the density of the catalytic active site and leading to a decrease in ORR activity. The exact active site is still uncertain.

As discussed above, the Fe−N/C catalyst obtained from 800 °C heat-treatment was the most active ORR catalyst. Therefore, the catalyst obtained at 800 °C heat-treatment was used for all further studies.

### 3.4. Role of TPY content on ORR activity

Wang's research showed that the ratio of Fe to ligand in the precursor complex had a strong effect on the activity of the resulting catalyst [37]. So, five Fe−N/C catalysts with different mole ratios of Fe/TPY (1:2.1, 1:4, 1:5, 1:6 and 1:8) were synthesized and the polarization curves of each are presented in Fig. 7a. As a com- parison, Fig. 7b shows the ORR potentials at a current density of 0.5 mA cm$^{-2}$ as a function of the Fe to TPY ratio. It is revealed that as

the Fe to TPY ratio decreases the ORR potential of the corresponding catalyst is enhanced up to the ratio of 1:5, at which point it starts to fall off. Thus, 1:5 should be the optimal ratio. Wang et al. thought that the improvement in the ORR activity observed here was mainly due to the increase in Fe−N$_x$ active site density. When the Fe to TPY ratio decreases from 1:5 to 1:8, a decline in the ORR activity is also observed. This is attributed to the formation of more Fe−N$_4$ sites, which are less active than Fe−N$_2$ sites, and probably leads to a catalyst with reduced ORR activity [37]. In addition, we propose that the excessive ligands block the porous carbon and reduce the electronic conductivity of the catalyst providing another possible explanation for the decrease in ORR activity.

### 3.5. Effect of metal loading on ORR activity

To evaluate the effect of Fe loading on ORR activity, five Fe−N/C catalysts with Fe loadings of 3.0, 4.0, 5.0, 6.0 and 7.0 wt% were prepared by heat-treatment of Fe−TPY/C (mole ratio of Fe/TPY was 1:5) complex at 800 °C. The current-potential curves of these
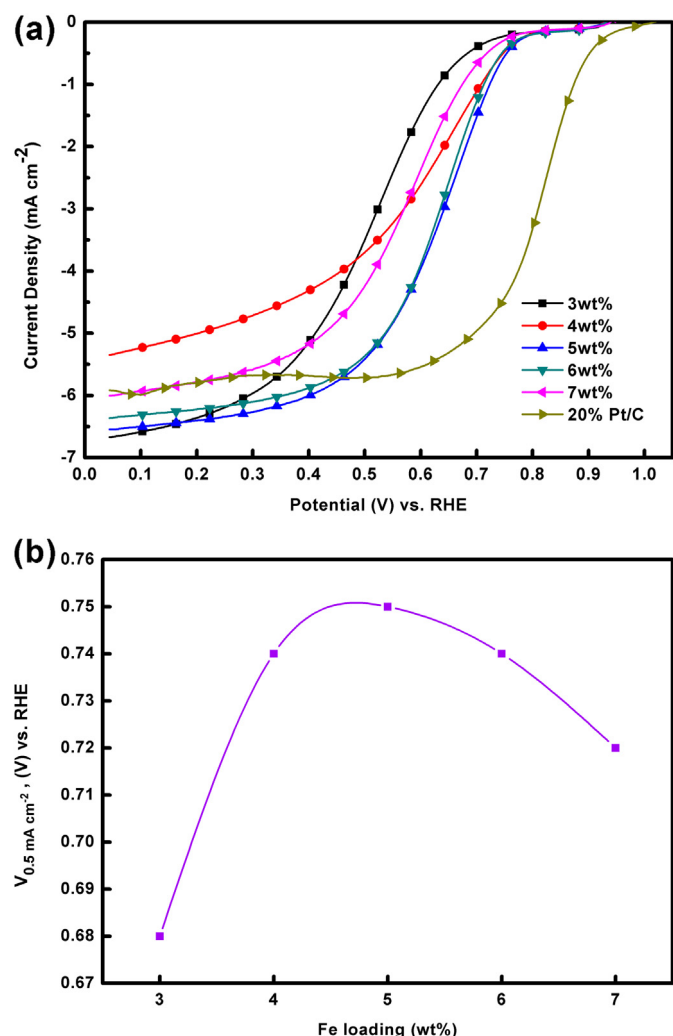
**Fig. 10.** Tafel plots according to Eq. (1). Date from Fig. 9.



**Fig. 8.** (a) Current–potential curves recorded on a rotating GC electrode coated with Fe–N/C catalysts having various Fe loadings as marked in the figure. Electrolyte: $O_2$-saturated 0.5 M $H_2SO_4$ solution; electrode rotation rate: 2500 rpm; potential scan rate: 5 mV s$^{-1}$; Fe–N/C catalyst loadings: 0.40 mg cm$^{-2}$. (b) ORR potential at 0.5 mA cm$^{-2}$ as a function of Fe loading in the catalyst.
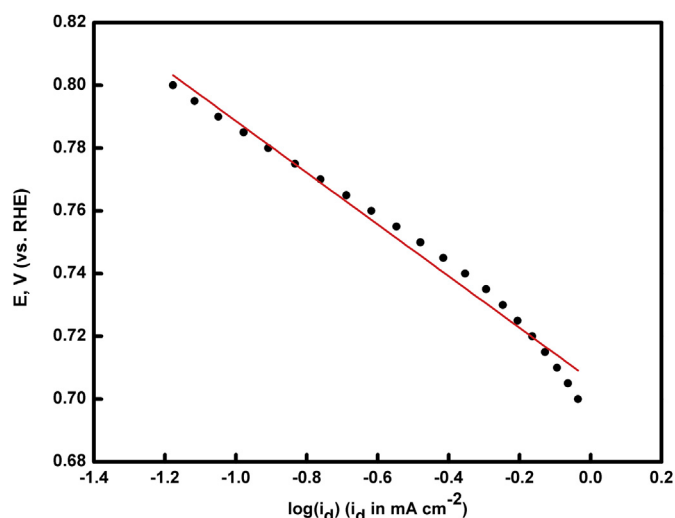
catalysts are shown in Fig. 8a and the curve of the 20 wt% Pt/C (ETEK) catalyst is also plotted for comparison. The ORR potentials at a current density of 0.5 mA cm$^{-2}$ plotted as a function of Fe loadings (data taken from Fig. 8a) are shown in Fig. 8b. From the data in this figure, it is clearly observed that at first the catalytic ORR potential increased with increasing Fe loading but fell off when the Fe content is greater than 5 wt%. The optimal Fe loading with the highest potential at 0.5 mA cm$^{-2}$ is 5 wt%. It is still unclear why the ORR activity decreases when the Fe loading exceeds 5 wt%. Zhang et al. [38] detected that metallic Fe and/or carbidic Fe aggregates were formed when the Fe loading was higher than 5 wt%. This metallic Fe and/or carbidic Fe aggregation can occur near and at the top of ORR active Fe–N sites thereby changing the nature of the active sites and thus blocking $O_2$ access to them. This is the cause of reduction in the ORR kinetic activity resulting in a reduced potential at 0.5 mA cm$^{-2}$ as shown in Fig. 8b. As shown in Fig. 8a, the current Fe-based catalyst (Fe–N/C) is still inferior to the Pt based catalysts (Pt/C) due to an unknown reason.
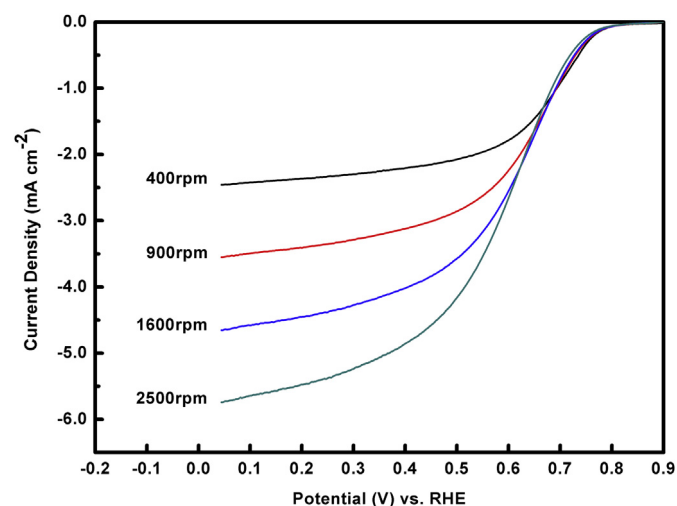


**Fig. 9.** Current–voltage curves for the ORR on a GC electrode coated with Fe–N/C catalyst. Recorded in a 0.5 M $H_2SO_4$ solution at various electrode rotation rates. Potential scan rate: 5 mV s$^{-1}$; Fe–N/C loading in the catalyst coating: 0.40 mg cm$^{-2}$.
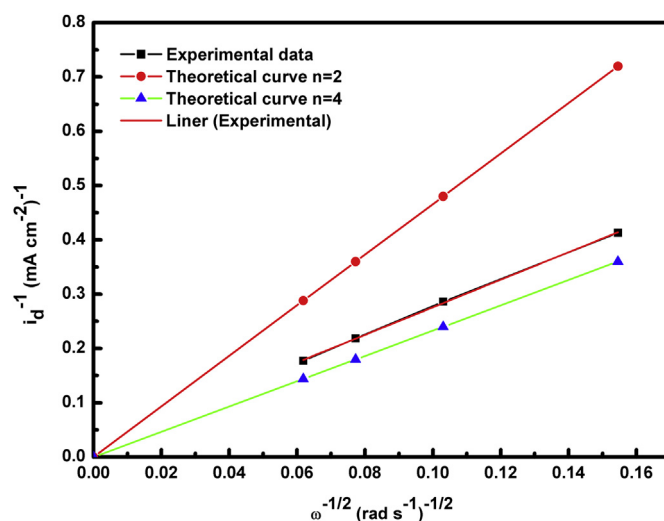


**Fig. 11.** Koutecky–Levich plots for the ORR on a Fe–N/C coated GC electrode. The current density data were taken at 0.1 V (vs. RHE) from Fig. 7. Theoretical plots for 2- and 4-electron transfer reactions are also shown.

### 3.6. Kinetic study of the ORR catalyzed by pyrolyzed Fe–N/C catalysts

In order to evaluate the kinetic parameters of the current-potential curves, one of the Fe–N/C catalysts with Fe loading of 5 wt% obtained via heat-treatment of the Fe-TPY/C (mole ratio of Fe/TPY was 1:5) complex at 800 °C were recorded at various electrode rotation rates from 400 to 2500 rpm in an $O_2$-saturated 0.5 M $H_2SO_4$ solution (shown in Fig. 9). The curves are similar to the results reported in our previous paper [9]. The curves do not show well-defined limiting current plateaus particularly at higher rotation rates.

As discussed in the literature [9,10], the current densities in the low over potential (such as narrow potential range of 0.7–0.8 V vs. RHE) are purely electrochemical kinetic current densities. However,

the current densities in the potential range <0.7 V are affected by both electrochemical kinetic and $O_2$ diffusion currents. Therefore, the relationship between the electrode potential and the current density in the low over potential range (i.e. 0.7–0.8 V) can be expressed as a Tafel equation (Eq. (1)),

$$E = E^0 + 2.303RT\log\left(i^0\right)/\alpha n_\alpha F - 2.303RT\log(i_d)/\alpha n_\alpha F \qquad (1)$$

where $E$ is the applied electrode potential, $E^0$ is the thermodynamic electrode potential under the measurement conditions ($E^0 = 1.23$ V vs. RHE), $i^0$ is the exchange current density, $i_d$ is the measured ORR current density, $R$ is the universal gas constant (8.314 J mol$^{-1}$ K$^{-1}$), $F$ is Faraday's constant (96,487 C mol$^{-1}$), $T$ is the absolute
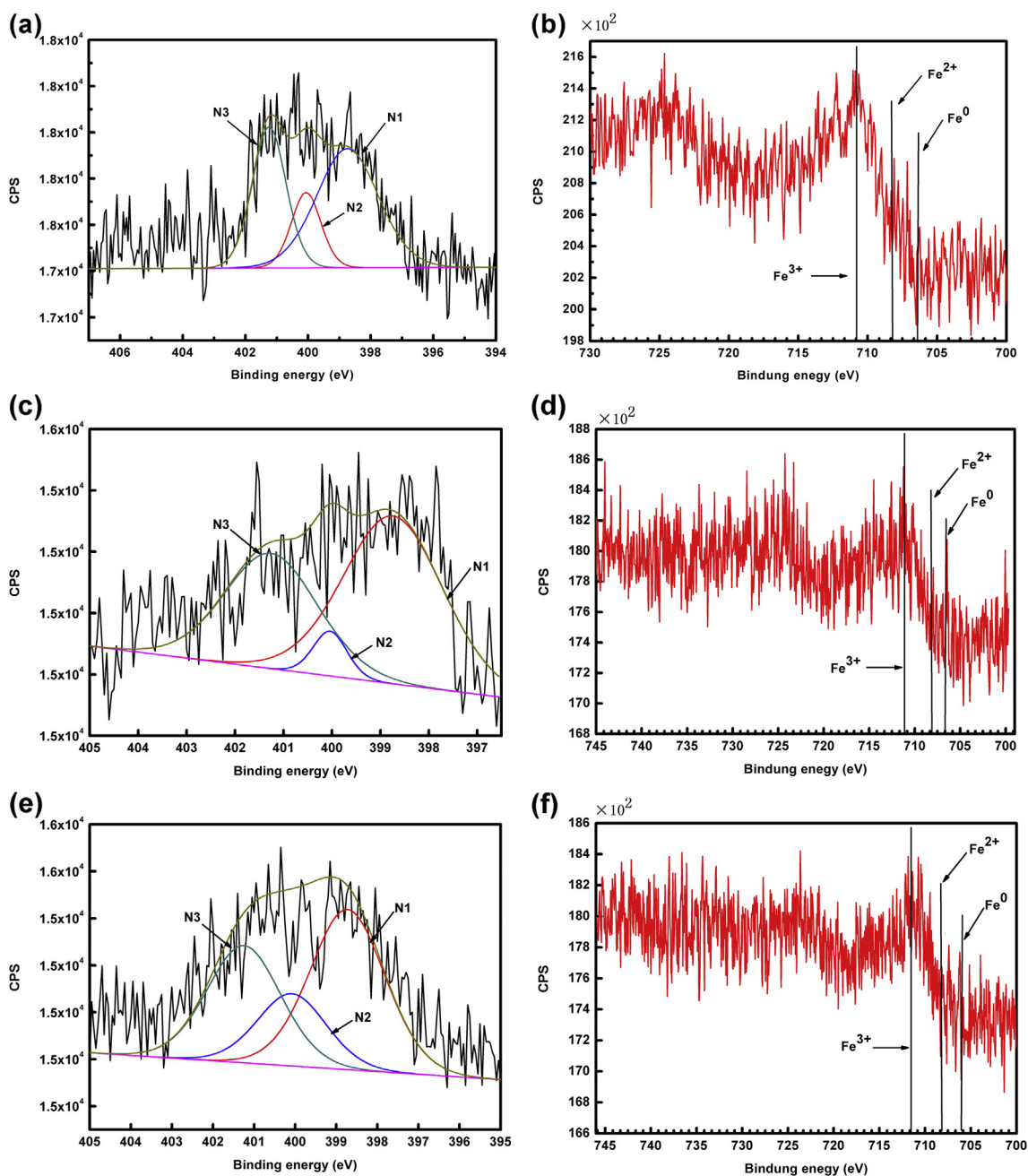


**Fig. 12.** XPS narrow-scan spectra of Fe-TPY/C sample heat-treated at 800 °C with mole ratio of (a) and (b) 1:2.1, (c) and (d) 1:5, (e) and (f) 1:8 for N1s and Fe2p levels. N1: pyridinic N; N2: pyrrolic N; N3: quaternary N (graphitic nitrogen). The bonding energies for the Fe2p$^{3/2}$ bond corresponding to Fe (0), Fe (II), and Fe (III) are highlighted. The Fe loading and heat-treatment temperatures of all samples are 5 wt% and 800 °C respectively.

temperature (298.15 K for our experimental conditions), $\alpha$ is the electron transfer coefficient in the rate determining step (RDS) of the ORR and $n_\alpha$ is the electron transfer number in the RDS (for the ORR process on an electrode, the $n_\alpha$ in the RDS is taken to be 1). The plotting of $E$ as a function of $\log(i_d)$ is shown in Fig. 10. The Tafel slope $(=2.303RT/\alpha n_\alpha F)$ and the intercept $(=E^0+(2.303RT/\alpha n_\alpha F)\log(i^0))$ are determined from the plot which allows us to calculate two important ORR kinetic parameters (the electron transfer coefficient, $\alpha = 0.72$ and the exchange current density, $i^0 = 4.4 \times 10^{-10}$ A cm$^{-2}$).

According to the Koutecky–Levich theory, the overall electron transfer number can be evaluated based on current densities in the low potential range (0.1 V vs. RHE). The disk current density $(i_d)$ on the RDE can be expressed as Eq. (2),

$$1/i_d = 1/i_k + i/0.62nFC_{O_2}(D_{O_2})^{2/3}\nu^{-1/6}\omega^{-1/2} \qquad (2)$$

where $i_k$ is the kinetic current density of the ORR, $n$ is the overall electron transfer number in the ORR, $F$ is Faraday's constant as defined in Eq. (1), $C_{O_2}$ is the $O_2$ concentration in the aqueous solution (mol cm$^{-3}$), $D_{O_2}$ is the $O_2$ diffusion coefficient (cm$^2$ s$^{-1}$), $\nu$ is the kinetic viscosity of the electrolyte (0.01 cm$^2$ s$^{-1}$) and $\omega$ is the electrode rotation rate (rad s$^{-1}$). According to Eq. (2), the Plot of $1/i_d$ as a function of $\omega^{-1/2}$ can give the overall electron transfer number $(n)$ if the values of $C_{O_2}$, $D_{O_2}$ and $\nu$ are known. Fig. 11 shows the Koutecky–Levich plots for the experimental data at 0.1 V and the theoretical plots for 2- and 4-electron transfer ORR processes. By calculating the slope of the reaction, the electron transfer number in the overall reduction process can be obtained as 3.7, suggesting that the catalyzed ORR by the Fe-TPY/C catalyst after 800 °C heat-treatment is mainly a 4-electron transfer pathway from $O_2$ to water.

### 3.7. XPS analysis of the Fe−N/C catalysts

In order to obtain additional information about the active sites of the catalysts, XPS narrow-scan spectra of Fe-TPY/C samples heat-treated at 800 °C with mole ratios of 1:2.1, 1:5, and 1:8, for N1s and Fe2p$^{2/3}$ levels are shown in Fig. 12. The N1s peaks can be separated into three components centered near the binding energies of 398.74 eV (N1), 400.03 eV (N2) and 401.26 eV (N3). The N1s peak at 398.74 eV could be assigned to the pyridinic type nitrogen, which consists of one N atom at the edge of a graphene layer contributing 1-electron to the π bonding [19]. N$_2$ might correspond to the pyrrolic N and N1s peak at 401.26 eV can be attributed to quaternary N (graphitic nitrogen), which replaced the central C atoms in graphene layers [39]. The well-defined graphitic structure formed during the heat-treatment of Fe-TPY/C is observed in HRTEM images (Fig. 4b). Wu et al. [5] thought that these graphene sheets correlated to the high activity of Fe−N/C type catalysts. The total and different types of N atomic percentages of these catalysts are listed in Table 1. Although the content of total N in the catalyst with mole ratio of 1:8 is much higher than that of 1:2.1, their ORR catalytic activities are similar. This indicates that the content of total N is not in proportion to the catalytic activity. This conclusion can be strengthened by data showing that the catalysts with mole ratios of 1:2.1 and 1:5, and therefore the lowest and highest catalytic activity, have the same total N content as indicated by XPS. A further

**Table 1**
The N atomic percentage of catalysts with different mole ratio of Fe/TPY.

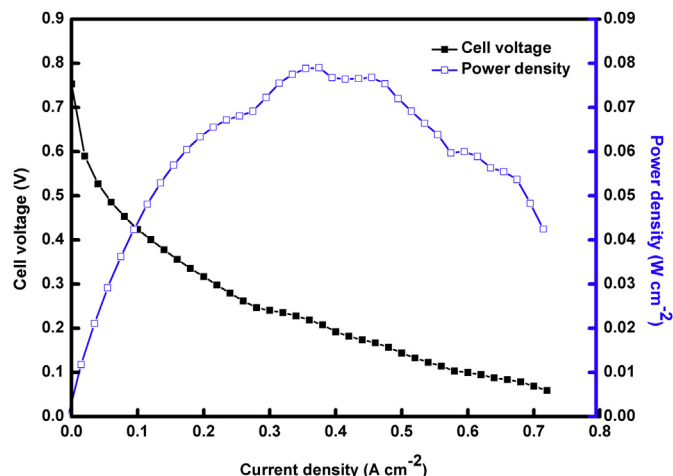| Mole ratio of Fe/TPY | Total N atomic (At. %) | N1 (At. %) | N2 (At. %) | N3 (At. %) |
|---|---|---|---|---|
| 1:2.1 | 0.86 | 0.44 | 0.13 | 0.29 |
| 1:5 | 0.86 | 0.50 | 0.04 | 0.32 |
| 1:8 | 1.12 | 0.52 | 0.22 | 0.38 |



**Fig. 13.** Polarization and power density curves at 60 °C for $H_2$ and $O_2$ PEMFC with 800 °C heat-treated Fe-TPY/C as the cathode catalyst. MEA active area 25.0 cm$^2$, Cathode catalyst loading 7.98 mg cm$^{-2}$ of Fe−N/C, and anode catalyst loading 0.4 mg cm$^{-2}$ 20 wt% Pt/C, Membrane was Nafion 112. Hydrogen flow rate 0.5 L min$^{-1}$ and oxygen flow rate 0.8 L min$^{-1}$. Fuel cell operated at 100% relative humidity and no backpressure.

comparison of the percentages of different types of N shows that the catalyst with the mole ratio of 1:5 contains more pyridinic and graphitic nitrogen, and has the highest catalytic activity. This indicates that the atomic N contributing to the ORR catalytic activity of Fe−N/C catalysts may be pyridinic nitrogen and graphitic nitrogen.

The XPS narrow-scan spectra for Fe2p$^{2/3}$ are also shown in Fig. 12. The median values of these energies are displayed in the spectra as vertical lines. According to the literature [10] the binding energies for Fe2p$^{3/2}$ of Fe (0), Fe (II), and Fe (III) are 706.7−707.2 eV, 707.1−708.7 eV and 710.8−711.8 eV, respectively. The standard Fe2p$^{2/3}$ signals for metallic iron, ferrous and ferric states were located at 707 eV, 708 eV and 711 eV, respectively. After comparing the Fe2p$^{2/3}$ peak positions with these standard binding energies, it can be concluded that the ferric state is the dominant species on all Fe−N/C catalysts. The presence of Fe (III) should be due to the conversion of Fe (II) irons coming from the starting material used in the synthesis. These Fe$^{3+}$ species can be Fe (III)−N$_x$, Fe (III) carbide or Fe (III) oxides.

### 3.8. Evaluation of catalyst activity in a PEMFC

To evaluate the ORR catalytic activity of the Fe−N/C catalyst in practical fuel cell applications, membrane electrode assemblies (MEAs) were fabricated with an 800 °C heat-treated Fe-TPY/C catalyst as the cathode. A PEMFC assembled with such an MEA was tested using a fuel cell test station. Backpressure was not applied to the MEA for both $H_2$ and $O_2$. Fig. 13 shows the polarization curves and the corresponding power density curves obtained at 60 °C. The open circuit voltage is around 0.75 V. At a cell voltage of 0.21 V, the current density is 0.38 A cm$^{-2}$ with a maximum power density of 0.08 W cm$^{-2}$. This result is better than that of iron TPTZ composite cathode catalysts in fuel cell performance developed by Bezerra [19] with a backpressure of 3.04 atm. The results reported in this work function to make the non-noble metal catalysts one step closer to commercialization.

### 4. Conclusion

TPY was selected as one N-containing precursor to prepare carbon-supported Fe−TPY complexes for the purpose of developing

a new ORR catalyst. The complexes were then heat-treated at temperatures ranging from 600 °C to 900 °C to synthesize Fe–N/C catalysts. The catalyst with a Fe loading of 5 wt% obtained via heat-treated Fe–TPY/C (mole ratio of Fe/TPY was 1:5) complex at 800 °C shows the highest ORR activity. The overall electron transfer number is calculated to be 3.7, suggesting that the catalyzed ORR by the Fe–TPY/C catalyst after being heat-treated at 800 °C is mainly a 4-electron transfer pathway from $O_2$ to water. The result of XPS indicates that the main atomic N contributing to catalytic activity towards ORR of Fe–N/C catalyst may be from pyridinic nitrogen and graphitic nitrogen. At a cell voltage of 0.21 V the single cell test results show a current density of 0.38 A cm$^{-2}$ with a power density of 0.08 W cm$^{-2}$ at 60 °C without backpressure. This makes the non-noble metal catalysts one step closer to commercialization.

## Acknowledgements

## References

[1] Y. Feng, N. Alonso-Vante, Phys. Stat. Sol.(b) 245 (2008) 1792–1806.
[2] A. Velázquez-Palenzuela, L. Zhang, L.C. Wang, P.L. Cobot, E. Brillas, K. Tsay, J. Zhang, Electrochim. Acta 56 (2011) 4744–4752.
[3] C.W.B. Bezerra, L. Zhang, K. Lee, H. Liu, A.L.B. Marques, E.P. Marques, H. Wang, J. Zhang, Electrochim. Acta 53 (2008) 4937–4951.
[4] L. Zhang, J. Zhang, D.P. Wilkinson, H. Wang, J. Power Sources 156 (2006) 171–182.
[5] G. Wu, K.L. More, C.M. Johnston, P. Zelenay, Science 332 (2011) 443–447.
[6] J. Herranz, F. Jaougn, M. Lefevre, U.I. Kramm, E. Proiett, J. Dodelet, P. Bogdanoff, S. Fiechter, I. Abs-Wurmbach, P. Bertrand, T.M. Arruda, S. Mukejee, J. Phys. Chem. C 115 (2011) 16087–16097.
[7] E. Proietti, F. Jaouen, M. Lefevre, N. Larouche, J. Tian, J. Herranz, J. Dodelet, Nat. Commun. 2 (2011) 416–427.
[8] F. Jaouen, J. Herranz, M. Lefevre, J. Dodelet, U.I. Kramm, I. Herrmann, P. Bogdanoff, J. Maruyama, T. Nagaoka, A. Garsuch, J.R. Dahn, T. Olson, S. Pylypenko, P. Atanassov, E.A. Ustinov, ACS Appl. Maters. Interfaces 1 (2009) 1623–1639.
[9] S. Li, L. Zhang, H. Liu, M. Pan, L. Zan, J. Zhang, Electrochim. Acta 55 (2010) 4403–4411.
[10] S. Li, L. Zhang, J. Kin, M. Pan, Z. Shi, J. Zhang, Electrochim. Acta 55 (2010) 7346–7353.
[11] N.A. Vante, W. Jaegermann, H. Tributsch, W. Honle, K. Yvon, J. Am. Chem. Soc. 109 (1987) 3251–3257.
[12] N. Alonso-Vante, H. Tributsch, O. Solorza-Feria, Electrochim. Acta 40 (1995) 567–576.
[13] A. Titov, P. Zapol, P. Kral, D. Liu, H. Iddir, K. Baishya, L.A. Curtiss, J. Phys. Chem. C 113 (2009) 21629–21634.
[14] K. Gong, F. Du, Z. Xia, M. Durstock, L. Dai, Science 323 (2009) 760–764.
[15] R. Liu, D. Wu, X. Feng, K. Miillen, Angew. Chem. Int. Ed. 49 (2010) 2565–2569.
[16] G. Liu, X. Li, P. Ganesan, B.N. Popov, Appl. Catal. B Environ. 93 (2009) 156–165.
[17] L. Zhang, Z. Xia, J. Phys. Chem. C 115 (2011) 11170–11176.
[18] K.R. Lee, K.U. Lee, J.W. Lee, B.T. Ahn, S.I. Woo, Electrochem. Commun. 12 (2010) 1052–1055.
[19] C.W.B. Bezerra, L. Zhang, K. Lee, H. Liu, J. Zhang, Z. Shi, A.L.B. Marques, E.P. Marques, S. Wu, J. Zhang, Electrochim. Acta 53 (2008) 7703–7710.
[20] J. Choi, R.S. Hsu, Z. Chen, J. Phys. Chem. C 114 (2010) 8048–8053.
[21] N. Mano, J.E. Yoo, J. Tarver, Y. Loo, A. Heller, J. Am. Chem. Soc. 129 (2007) 7006–7007.
[22] G. Wu, Z. Chen, K. Artyushkova, F.H. Garzon, P. Zelenay, Eletrochem. Soc. 16 (2008) 159–170.
[23] M. Lefevre, E. Proietti, F. Jaouen, J. Dodelet, Science 324 (2009) 71–74.
[24] V. Bambagioni, C. Bianchini, J. Filippi, A. Lavacchi, W. Oberhauser, A. Marchionni, S. Moneti, F. Vizza, R. Psaro, V.D. Santo, A. Gallo, S. Recchia, L. Sordelli, J. Power Sources 196 (2011) 2519–2529.
[25] K. Lee, L. Zhang, H. Lui, R. Hui, Z. Shi, J. Zhang, Electrochim. Acta 54 (2009) 4704–4711.
[26] P.H. Matter, E. Wang, M. Arias, E.J. Biddinger, U.S. Ozkan, J. Phys. Chem. B 110 (2006) 18,374–18,384.
[27] R. Bashyam, P. Zelenay, Nature 443 (2006) 63–66.
[28] Y. Lee, H.J. Song, H.S. Shin, H.J. Shin, H.C. Choi, Small 1 (2005) 975–979.
[29] R. Fallahpour, Synthesis 2 (2003) 155–184.
[30] K. Ito, T. Nagata, K. Tanaka, Inorg. Chem. 40 (2001) 6331–6333.
[31] J. Limburg, J.S. Vrettos, L.M. Liable-Sands, A.L. Rheingold, R.H. Crabtree, G.W. Brudvig, Science 283 (1999) 1524–1527.
[32] F. Wang, G. Liu, B. Qian, Chin. J. Appl. Chem. 5 (1988) 15–20.
[33] M. Lundberg, M.R.A. Blomberg, P.E.M. Siegbahn, Inorg. Chem. 43 (2004) 264–274.
[34] Q. Yang, L. Wu, Z. Wu, L. Zhang, C. Tung, Inorg. Chem. 41 (2002) 5653–5655.
[35] T. Abea, M. Kaneko, J. Mol. Catal. A: Chem. 169 (2001) 177–183.
[36] C.W.B. Bezerra, L. Zhang, H. Liu, K. Lee, A.L.B. Marques, E.P. Marques, H. Wang, J. Zhang, J. Power Sources 173 (2007) 891–908.
[37] L. Wang, L. Zhang, J. Zhang, Electrochim. Acta 56 (2011) 5488–5492.
[38] L. Zhang, K. Lee, C.W.B. Bezerra, J. Zhang, J. Zhang, Electrochim. Acta 54 (2009) 6631–6636.
[39] H.R. Byon, J. Suntivich, Y. Shao-Horn, Chem. Mater. 23 (2011) 3421–3428.

## Glossary

*CV:* cyclic voltammetry
*DNA:* deoxyribose nucleic acid
*GC:* glassy carbon
*HOR:* hydrogen oxidation reaction
*HRTEM:* high resolution transmission electron microscopy
*LSV:* linear sweep voltammetry
*MEA:* membrane electrode assembly
*ORR:* oxygen reduction reaction
*PANI:* polyaniline
*PEMFC:* proton exchange membrane fuel cell
*RDE:* rotating disk electrode
*RHE:* standard hydrogen electrode
*SCE:* saturated calomel electrode
*TPTZ:* tripyridyl triazine
*TPY:* 2,6-Bis(2-pyridy)-pyridine
*XPS:* X-ray photoelectron spectroscopy
*XRD:* X-ray diffraction